NORSAR

ROYAL NORWEGIAN COUNCIL FOR SCIENTIFIC AND INDUSTRIAL RESEARCH

NORSAR Scientific Report No. 1-85/86

FINAL TECHNICAL SUMMARY

1 April - 30 September 1985

L. B. Loughran (ed.)

Kjeller, December 1985

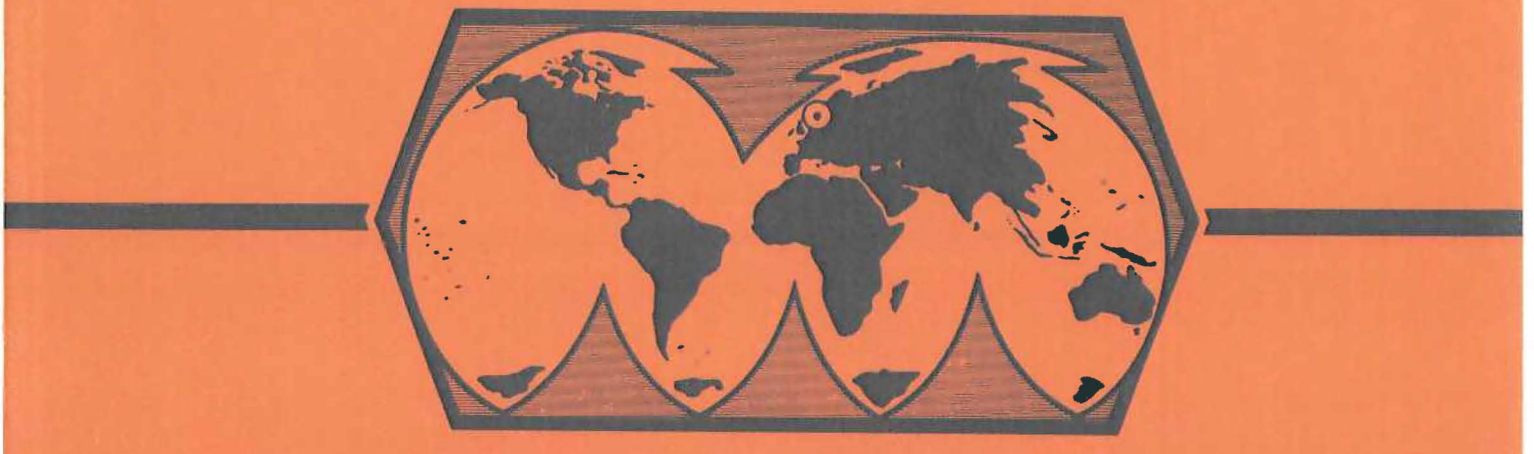

VII.3 Initial results from NORESS detection processing

Since January 1985 data from the new small-aperture array NORESS in Norway have been processed in real time at the NORSAR data center at Kjeller. The data used in the detection processing comprise 25 SPZ channels, deployed over an area 3 km in aperture and sampled at 40 Hz rate. The detection algorithm (RONAPP) has been described by Mykkeltveit and Bungum (1984), and the current implementation consists of

- Digital narrow-band filtering using a set of Butterworth recursive bandpass filters
- Beamforming, using both conventional and incoherent (envelope) beams
- A linear STA/LTA detector applied to each beam
- Frequency-wavenumber analysis of detected signals
- Association of regional phases to aid in locating events.

In the reporting period (April-September 1985), the RONAPP system has been operated with a fixed beam deployment, as summarized in Table VII.3.1. This deployment, which at the current stage is to be considered experimental, has been based upon the desire to obtain a balance between teleseismic and regional phase detection, within the limits of the processing system capability. Briefly, the current deployment is described as follows:

Beams 1-7 and beam 17 are infinite-velocity conventional beams with filter bands ranging from 1-3 Hz (beam 1) to 8-16 Hz (beam 7). For each of these beams, a subset of the array has been selected as shown in the table. Generally, the low-frequency beams have been formed from the outer rings (C and D), whereas the highest frequency beams are based on the inner (A and B) rings. It has previously been found (Mykkeltveit et al, 1985) that selecting such frequency-dependent subgeometries leads to

increased SNR relative to utilizing all sensors of the array in the beamforming.

Beams 8-16 are steered beams of typical teleseismic velocity (14 km/s), and variable azimuths and filter bands. All of these beams are steered towards Eurasia (azimuth range 0-180 deg), with the intention of providing improved teleseismic detection of the high-frequency signals seen from this area.

Beams 18-20 are incoherent (envelope) beams, which have been formed by filtering individual sensor traces and then adding the absolute values of the filtered traces with no time shift involved. As shown by Ringdal et al (1975), such beams are especially well suited for detecting signals of low coherency across the array. This would, for NORESS, typically occur for high frequency secondary phases.

We comment that the RONAPP package is very flexible with respect to beam deployment, within the overall limitation of 20 beams. Currently, the heavy filtering load involved in forming incoherent beams limits the number of such beams to 3, otherwise, it would have been desirable to include more high-frequency beams of this type. The threshold setting in the current RONAPP system has been somewhat conservative, in order to avoid extensive f-k processing of noise detections. In the near future, attempts will be made to allow for lower SNR thresholds.

In the following, we present some initial statistics on NORESS on-line detection results. These are based on the time period April-September 1985, and cover only those intervals (about 75 per cent of total time) when no significant land line transmission problems were encountered. Such problems were responsible both for occasional system outage and periods of large number of spike detections. It is noted here that the

satellite transmission of NORESS data to the U.S. has been conducted with minimal disruption in the period, thus the reliability of the NORESS field system has been excellent throughout.

Fig. VII.3.1 shows NORESS detections distributed by time of day (GMT). The most noteworthy feature is the large increase in overall detection numbers during daytime hours (local time is 1-2 hours different from GMT). This is clearly attributable to mining explosions, road work, etc., and the figure shows that the number of detected local and regional P phases (velocity 6-12.5 km/s) increases in the same proportion as the total detection numbers during daytime hours. In contrast, the number of detections with teleseismic P-velocities (>12.5 km/s) remains nearly independent of time of day. With the current parameter setting, there has in average been 102 NORESS detections per data-day, of which 25 are of estimated velocity 6-12.5 km/s and 18 of velocity >12.5 km/s.

In Fig. VII.3.2, NORESS detections are plotted by beam number. Note that in this, as well as the other statistics, only the beam with largest SNR is counted for each detection, and that the RONAPP processor groups detections together if they are separated in time by less than 4 seconds. From the figure we see that most of the detections with teleseismic phase velocities occur on beams 1-5, whereas the incoherent beams (18-20) represent almost exclusively detections with phase velocities <6 km/s (typical for secondary phases). A significant number of detections with low and intermediate phase velocities also occur on the high-frequency infinite velocity beams 5-7.

The distribution of NORESS detections by estimated azimuth is shown in Fig. VII.3.3. The concentration of detections in the azimuth interval 90-120 degrees is mostly associated with mining activity in central Sweden and western Russia. With regard to detections of estimated teleseismic velocity, the large majority

is in the range 0-120 degrees, covering mostly Asia. It should be noted that both the azimuth and velocity estimates computed by RONAPP have a fair amount of uncertainty, which must be taken into consideration. This will be further discussed in subsection VII.4.

Fig. VII.3.4 shows incremental and cumulative recurrence statistics for NORESS detections as a function of SNR. Coherent and incoherent (envelope) detections are plotted separately. For coherent beam detections, log N (N = number of detections) increases approximately linearly with decreasing log(SNR). On the other hand, the number of incoherent beam detections shows a sharp increase at low SNR values. This is partly because SNR of secondary phases almost always is very low, since the "noise" preceding such phases is the P-coda from the same event. However, preliminary review has also shown that the number of "noise" detections is significant for the envelope beams. Many of these have a very low apparent velocity (< 3 km/s), and procedures to eliminate such false alarms are currently being investigated.

In Fig. VII.3.5, we have subdivided the coherent beam detections into the three velocity intervals described earlier, and plotted separate recurrence statistics. For velocities < 6 km/s, the number of detections increases very sharply with decreasing SNR, again probably due to a predominance of low SNR secondary phases. (For coherent beams, there appears to be few instances of "noise" detections due to a conservative SNR setting.) The plots for intermediate and high velocity signals are similar, although the "slope" in the latter case is somewhat less steep. In either case, we do not see a sharp increase in the number of detections at low SNR, and this is consistent with the above assertion that

"noise" detections are essentially absent with the current RONAPP parameter setting.

In conclusion, the six-month period of RONAPP operation with fixed parameter setting has provided valuable statistical information which will now be used in incorporating improvements into the processing system. In parallel with this, results are now being obtained from a systematic review of NORESS bulletin output which has recently been initiated. Altogether, we plan, in the near future, to generate a new beam deployment, including possible lowering of the coherent beam SNR thresholds. The introduction of variable thresholds for incoherent beams (lower thresholds immediately following regional P detections) will be considered as a possibility to improve secondary phase detection, as will the possibility of masking "noise" detections with very slow phase velocities. Another planned refinement is to introduce a subroutine for faster f-k analysis, thus eliminating a serious bottleneck in the real-time processing, and to implement an interpolation procedure to obtain better precision in phase velocity and azimuth estimates than the current grid points allow. Finally, the regional signal characteristics discussed in subsections VII.7.1 and VII.7.2 will be taken into account in improving automatic phase association procedures.

F. Ringdal

References

Mykkeltveit, S. & H. Bungum (1984): Processing of regional seismic events using data from small-aperture arrays, Bull. Seism. Soc. Am., 74, 2313-2333.

Mykkeltveit, S., D.B. Harris & T. Kværna (1985): Preliminary evaluation of event detection and location capability of the small aperture NORESS array, NORSAR Semiannual Technical Summary, 1 Oct 84 - 31 Mar 85, NORSAR, Kjeller, Norway

Ringdal, F., E.S. Husebye & A. Dahle (1975): P-wave envelope representation in event detection using array data, IN: Exploitation of Seismograph Networks (E.G. Beauchamp, ed.), Nordhoff-Leiden.

********* NORESS ON-LINE BEAM DEPLOYMENT APR-SEPT 1985 *********

BEAM NO	AZI DEG	SLOW S/KM	FILTER BAND	BEAM TYPE	*** SP CHANNELS USED *** 1=USED, 0=UNUSED	STA/LTA THRESHOLD
1	0.	.000	1.0-3.0	C	100000000111111111111111	4.0
2	0.	.000	1.5-3.5	C	100000000111111111111111	4.0
3	0.	.000	2.0-4.0	C	100011111111111111111111	4.0
4	0.	.000	2.5-4.5	C	100011111111111000000000	4.0
5	0.	.000	3.0-5.0	C	100011111111111000000000	4.0
6	0.	.000	4.0-8.0	C	111111111000000000000000	5.0
7	0.	.000	8.0-16.	C	111111111000000000000000	5.0
8	0.	.070	2.0-4.0	C	100011111111111111111111	4.0
9	90.	.070	2.0-4.0	C	100011111111111111111111	4.0
10	180.	.070	2.0-4.0	C	100011111111111111111111	4.0
11	15.	.070	2.5-4.5	C	100011111111111111111111	4.0
12	75.	.070	2.5-4.5	C	100011111111111111111111	4.0
13	135.	.070	2.5-4.5	C	100011111111111111111111	4.0
14	25.	.070	3.0-5.0	C	100011111111111111111111	4.0
15	75.	.070	3.0-5.0	C	100011111111111111111111	4.0
16	125.	.070	3.0-5.0	C	100011111111111111111111	4.0
17	0.	.000	2.0-4.0	C	100011111111111000000000	4.0
18	0.	.000	1.0-2.0	I	100000000111111000000000	2.5
19	0.	.000	2.0-3.0	I	100000000111111000000000	2.5
20	0.	.000	2.0-4.0	I	100000000000000111111111	2.1

NOTE: BEAM TYPE 'C' MEANS COHERENT BEAM
'I' MEANS INCOHERENT (ENVELOPE) BEAM

THE CHANNEL SEQUENCE IS NORMAL: A0Z,A1Z-A3Z,B1Z-B5Z,C1Z-C7Z,D1Z-D9Z

Table VII.3.1 NORESS on-line processor beam deployment effective 14 March 1985.

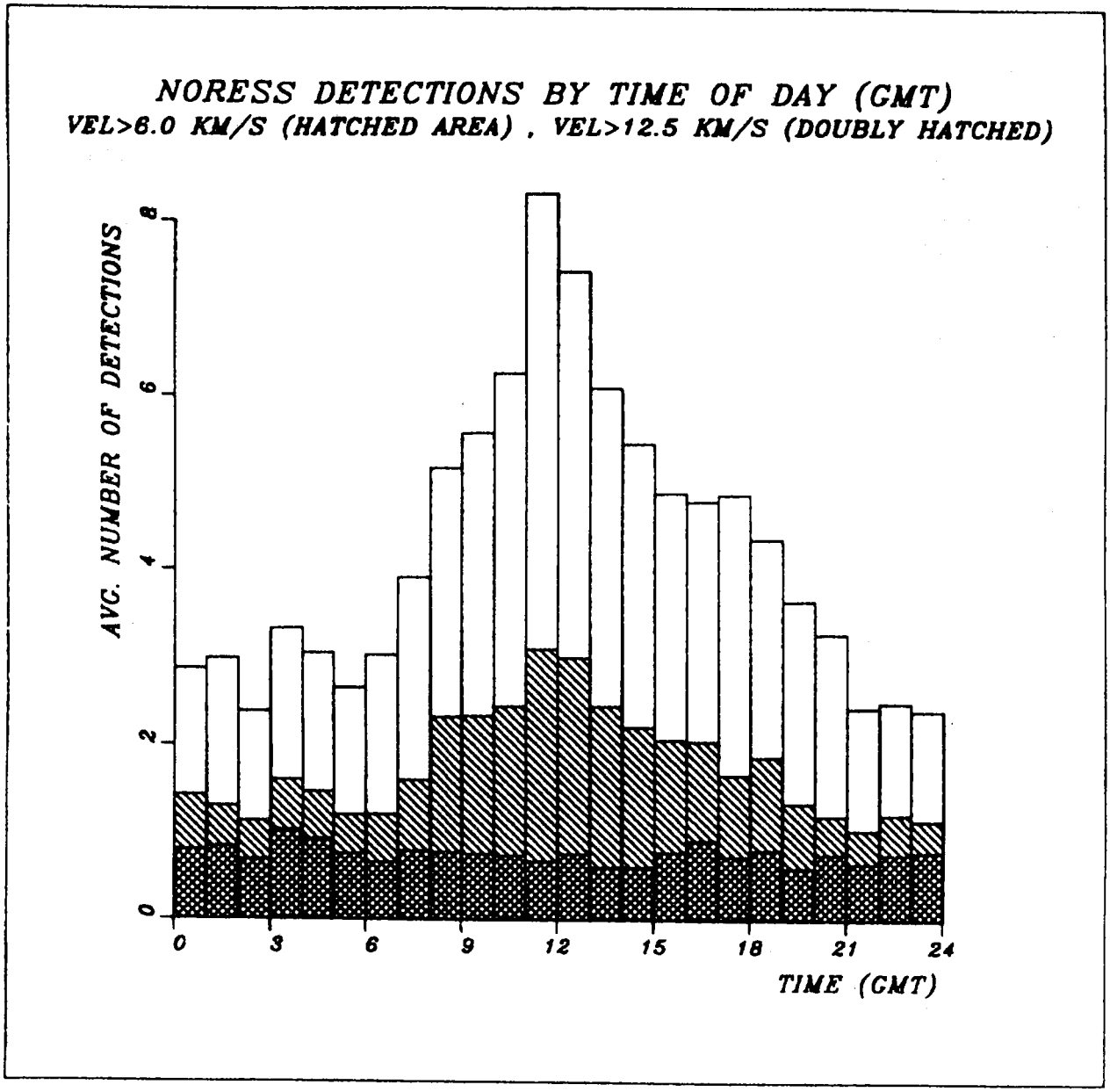

Fig. VII.3.1 Distribution of NORESS detections as a function of time of day (GMT). The average number of detections per hour is plotted, based on the time interval April-September 1985, with correction applied for system down times. The total heights of the columns correspond to all detections within the respective hours.
Unhatched ares: detections with estimated phase velocity < 6 km/s.
Singly hatched areas: detections with phase velocity between 6 and 12.5 km/s.
Doubly hatched areas: detections with phase velocity exceeding 12.5 km/s.

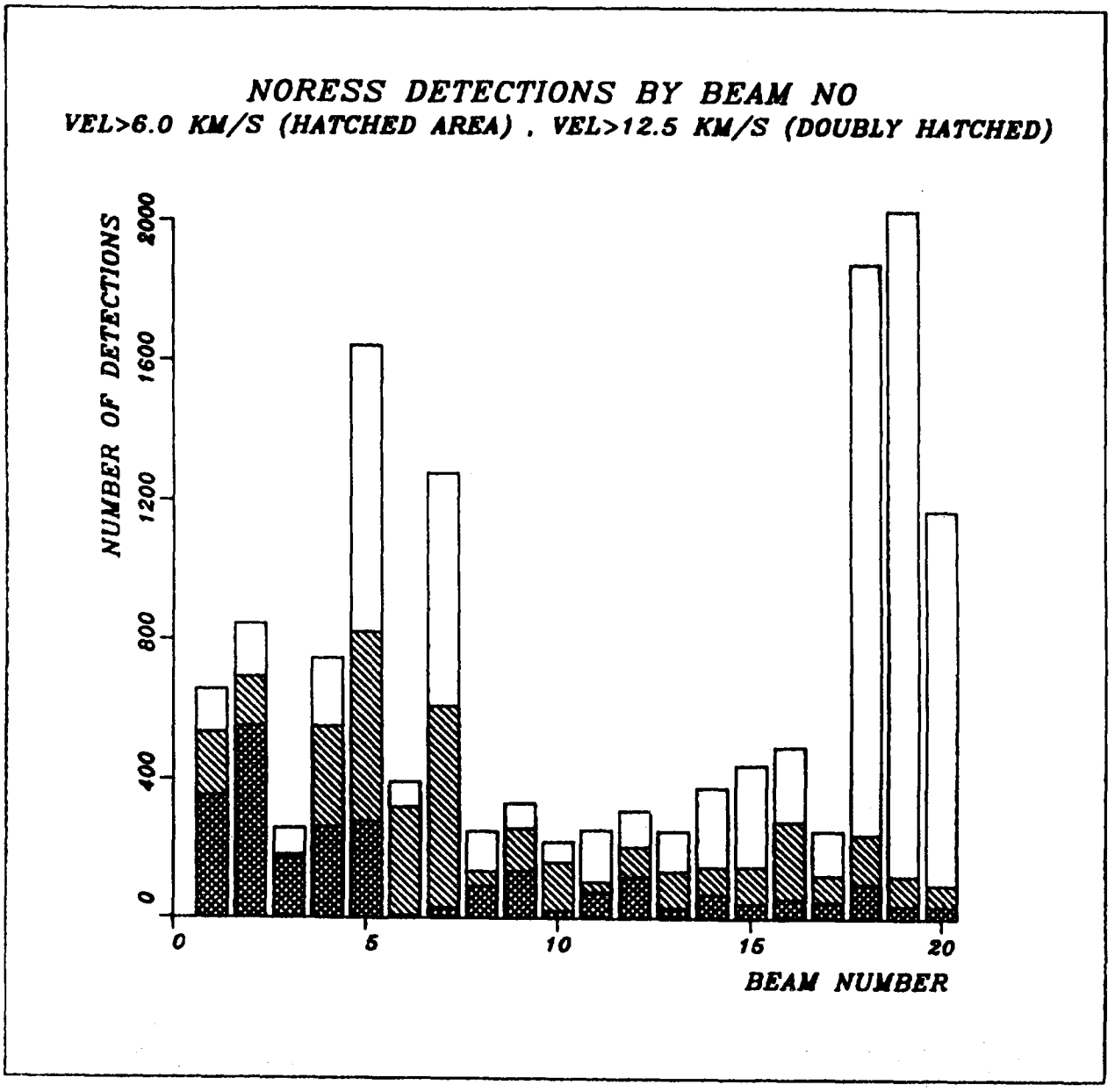

Fig. VII.3.2 NORESS detections during April-September 1985 distributed by beam number (see Table VII.3.1). For each detected phase, the beam with the largest SNR has been selected. The hatching convention is the same as in Fig. VII.3.1.

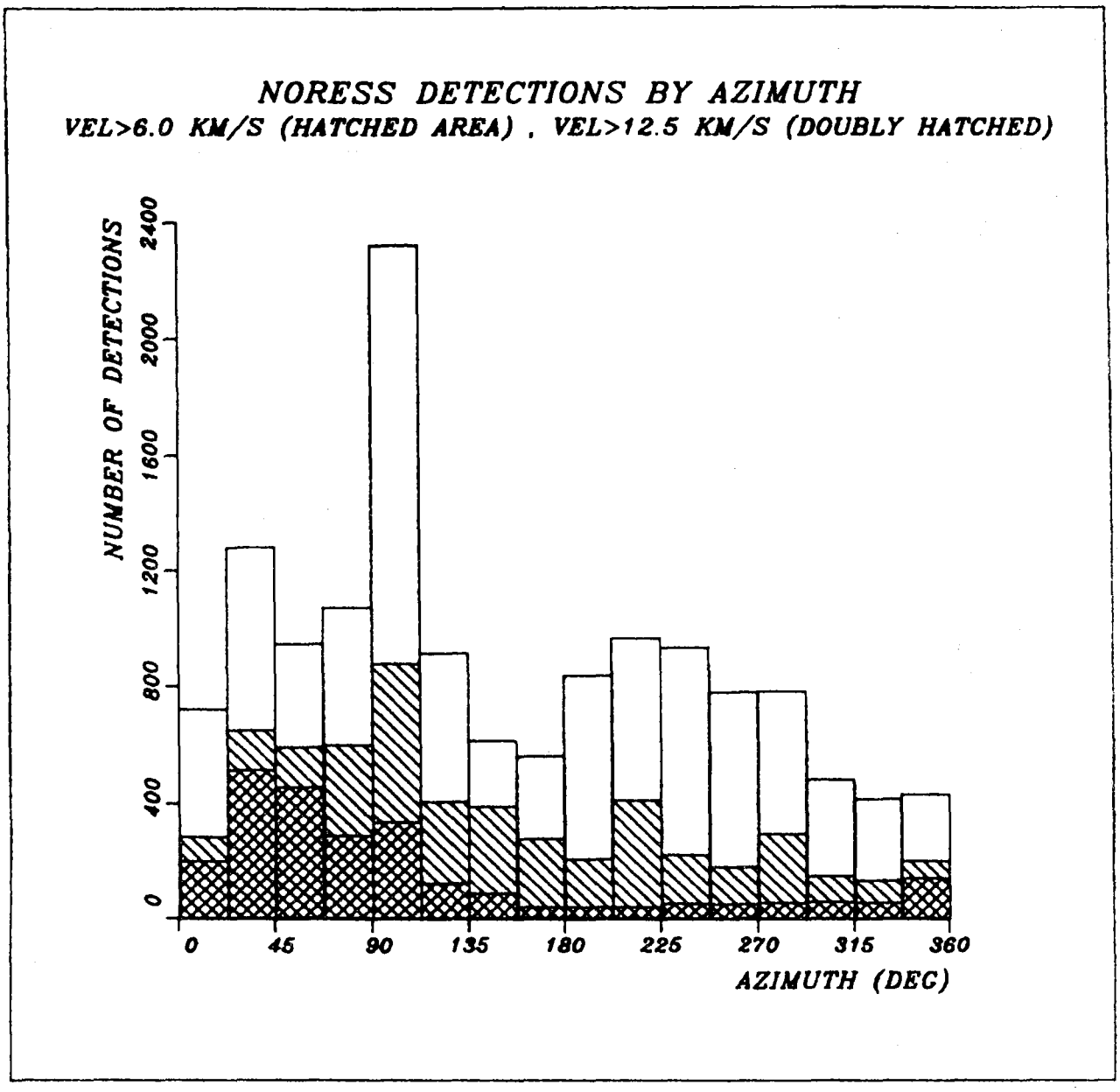

Fig. VII.3.3 NORESS detections during April-September 1985 as a function of estimated azimuth. The hatching convention is the same as in Fig. VII.3.1.

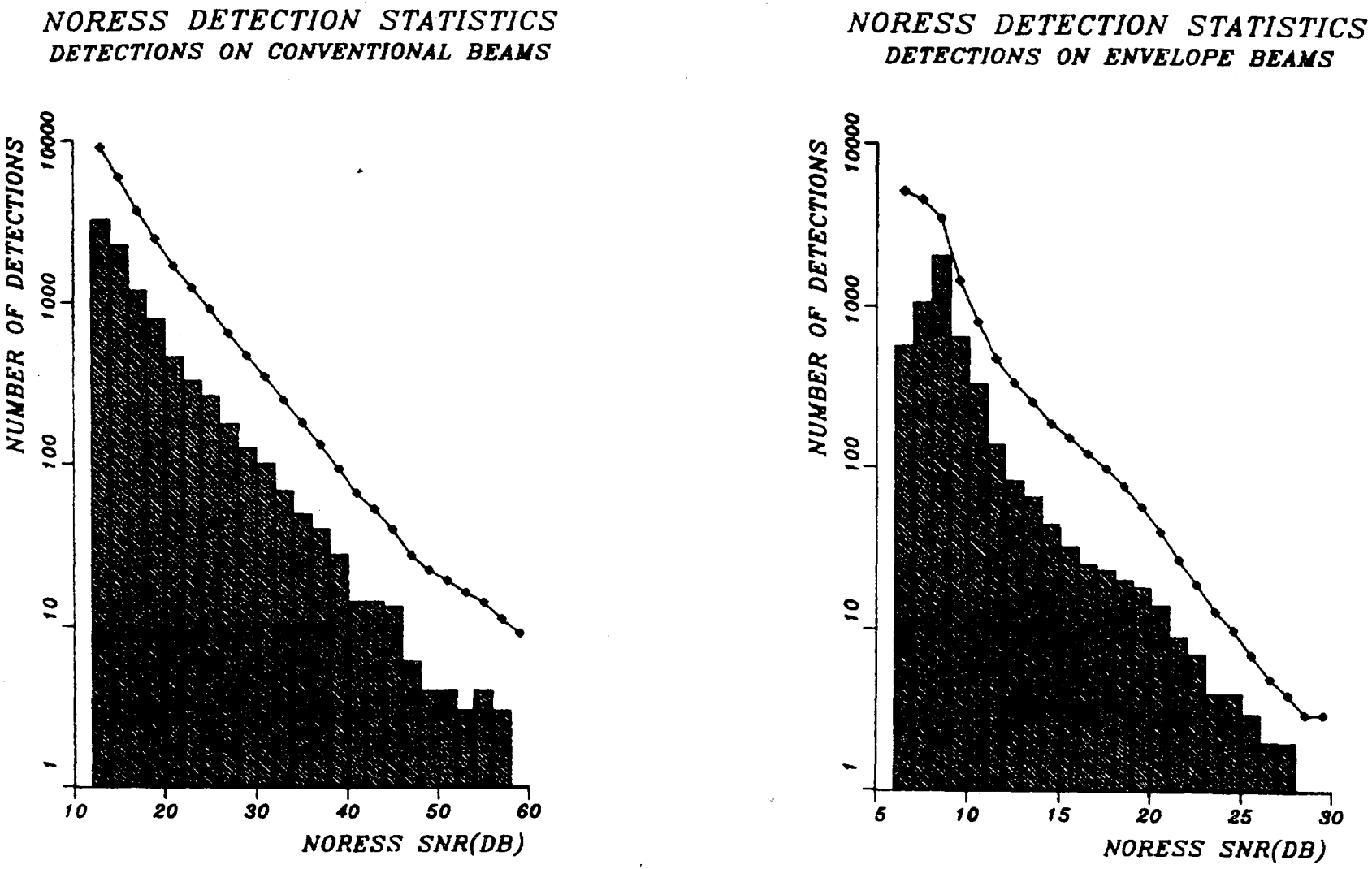

Fig. VII.3.4 NORESS detection statistics during April-September 1985 as a function of SNR. Incremental statistics (histograms) and cumulative statistics (lines) are plotted separately for all detections on conventional beams (nos. 1-17) and envelope beams (18-20) defined in Table VII.3.1. Note the differences in horizontal scales of the two plots.

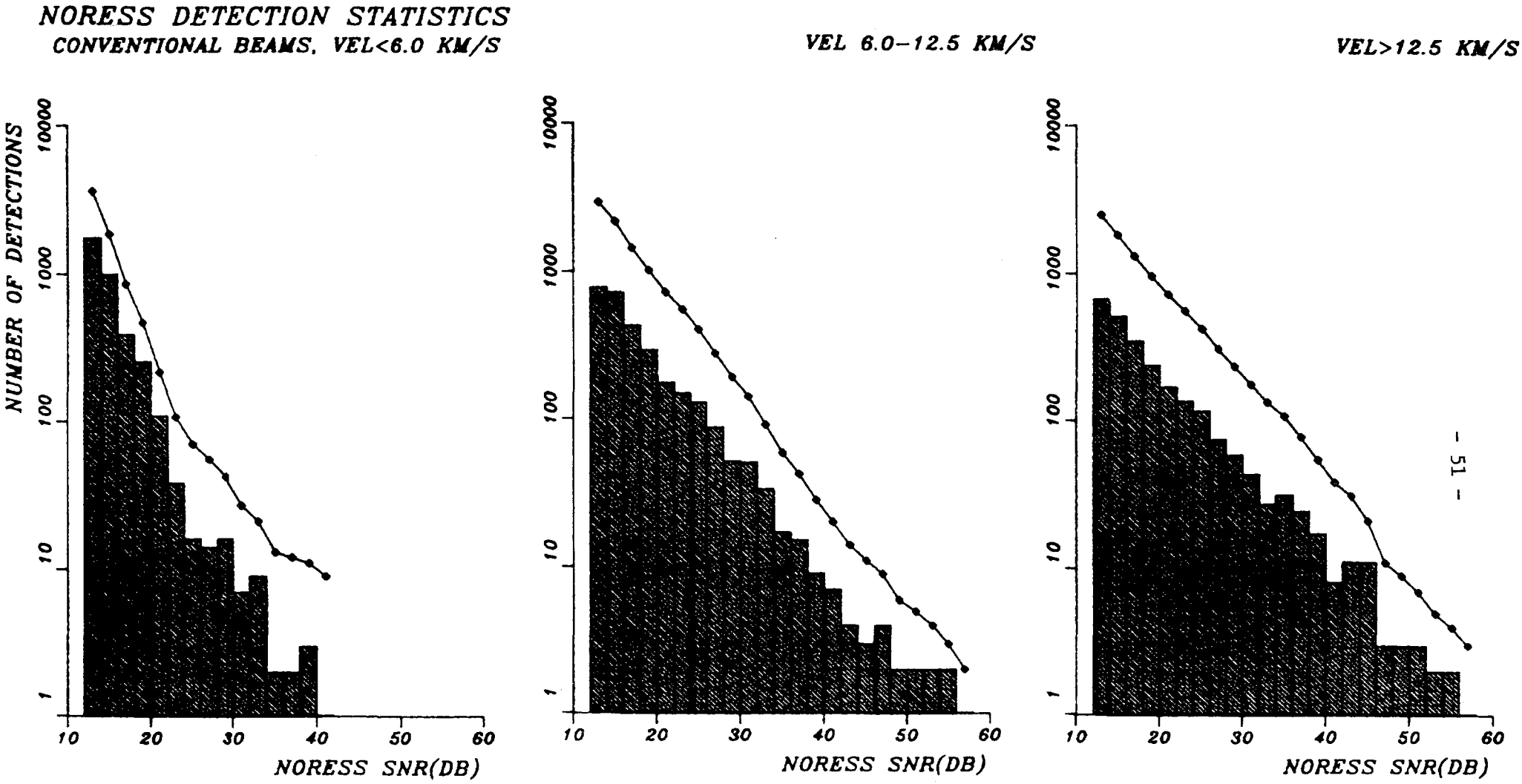

Fig. VII.3.5 NORESS detection statistics for conventional beams (nos. 1-17 of Table VII.3.1) in three velocity intervals (based on NORESS estimated phase velocity). The plots show incremental statistics (histograms) and cumulative statistics (lines). Note the differences in slopes of the logN vs SNR(DB) relations.